

Elucidating the Ordering in Self-Assembled Glycocalyx Mimicking Supramolecular Copolymers in Water

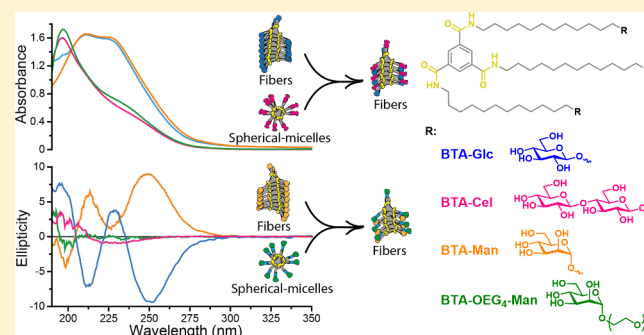
Simone I. S. Hendrikse,^{§,†} Lu Su,^{§,†} Tim P. Hogervorst,[‡] René P. M. Lafleur,[†] Xianwen Lou,[†] Gijbert A. van der Marel,[‡] Jeroen D. C. Codee,[‡] and E. W. Meijer^{*,†}

[†]Institute for Complex Molecular Systems, Eindhoven University of Technology, P.O. Box 513, 5600 MB Eindhoven, The Netherlands

[‡]Department of Bio-organic Synthesis, Leiden Institute of Chemistry, Leiden University, 2300 RA Leiden, The Netherlands

S Supporting Information

ABSTRACT: Polysaccharides present in the glycocalyx and extracellular matrix are highly important for a multitude of functions. Oligo- and polysaccharides-based biomaterials are being developed to mimic the glycocalyx, but the spatial functionalization of these polysaccharides represents a major challenge. In this paper, a series of benzene-1,3,5-tricarboxamide (BTA) based supramolecular monomers is designed and synthesized with mono- (BTA- β -D-glucose; BTA-Glc and BTA- α -D-mannose; BTA-Man) or disaccharides (BTA- β -D-cellobiose; BTA-Cel) at their periphery or a monosaccharide (BTA-OEG₄- α -D-mannose; BTA-OEG₄-Man) at the end of a tetraethylene glycol linker. These glycosylated BTAs have been used to generate supramolecular assemblies and it is shown that the nature of the carbohydrate appendage is crucial for the supramolecular (co)polymerization behavior. BTA-Glc and BTA-Man are shown to assemble into micrometers long 1D (bundled) fibers with opposite helicities, whereas BTA-Cel and BTA-OEG₄-Man formed small spherical micelles. The latter two monomers are used in a copolymerization approach with BTA-Glc, BTA-Man, or ethylene glycol BTA (BTA-OEG₄) to give 1D fibers with BTA-Cel or BTA-OEG₄-Man incorporated. Consequently, the carbohydrate appendage influences both the assembly behavior and the internal order. Using this approach it is possible to create 1D-fibers with adjustable saccharide densities exhibiting tailored dynamic exchange profiles. Furthermore, hydrogels with tunable mechanical properties can be achieved, opening up possibilities for the development of multicomponent functional biomaterials.



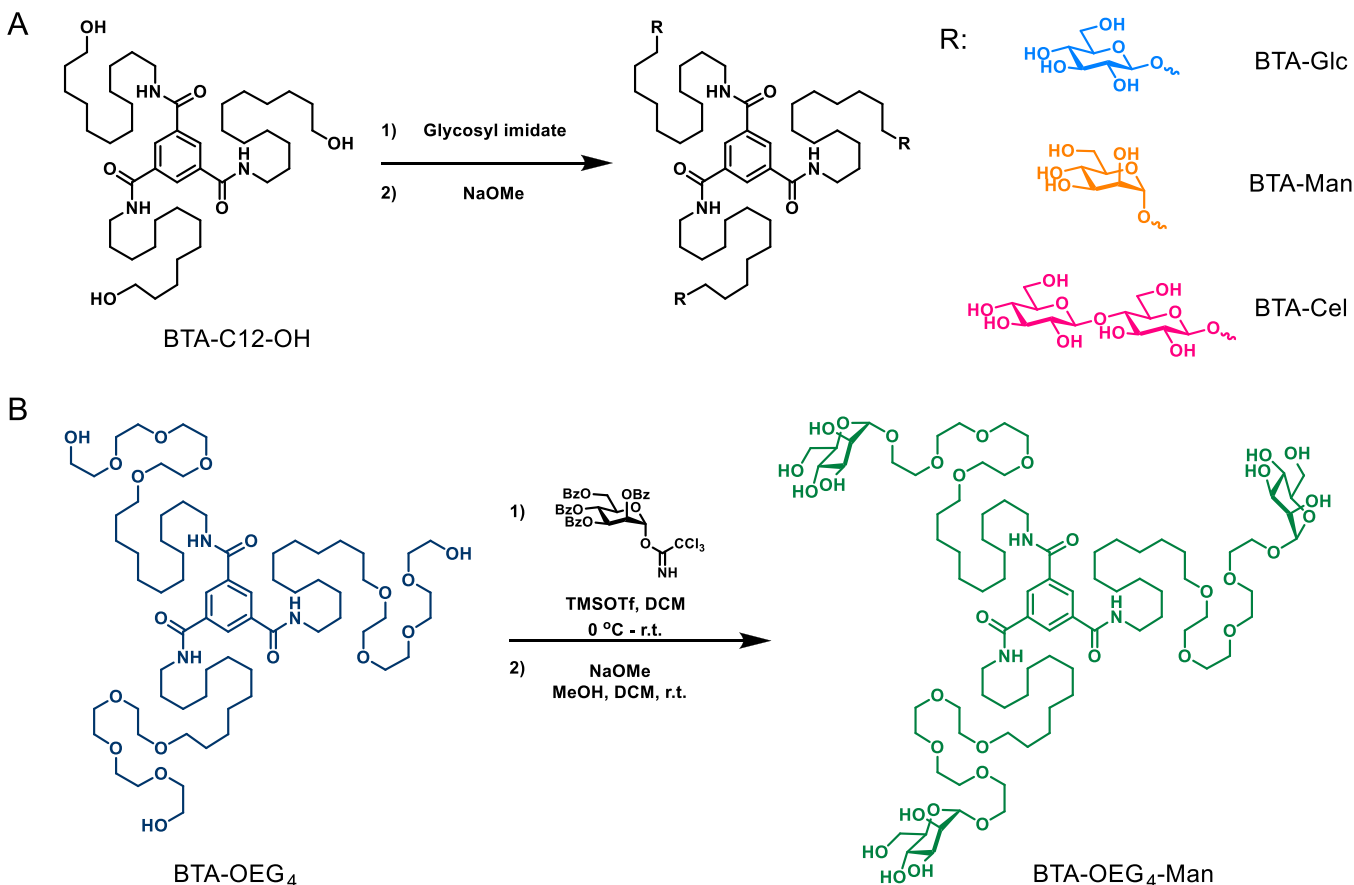
INTRODUCTION

Polysaccharides are abundantly present on the cell surface, i.e., the glycocalyx, and in the extracellular matrix, e.g., glycosaminoglycans (GAGs). They play a number of critical roles in many essential biological processes, both structurally and functionally,^{1,2} such as water immobilization, growth factor binding, cell attachment, and signaling.^{3–5} The multivalency effect—the cooperative action of multiple interaction simultaneously—is fundamental in many of these carbohydrate-receptor interactions.⁶ Since specificity and affinity binding are significantly influenced by the structural and spatial arrangement of the carbohydrate ligands in polysaccharides, synthetic glycopolymers and glycodendrimers serve as attractive candidates for biomaterials and they can be used to investigate interaction mechanisms underlying biological events.^{7–9} However, the synthesis of stereo-, composition-, and sequence-defined glycopolymers or glycodendrimers generally requires multiple steps, making it challenging and time-consuming. Additionally, it is hard to achieve adaptive rearrangements in the polymers and therefore, assembled structures, e.g., supramolecular copolymers, are seen as attractive alternatives.

Inspired by the architectures obtained through self-organization of biological macromolecules into complex but highly ordered matter, supramolecular polymers attained much attention due to their resemblance in self-assembled properties.^{10,11} Dynamic, adaptable, and responsive supramolecular materials, including supramolecular glycopolymers, can be formed from monomeric building blocks exploiting non-covalent interactions in the form of hydrophobic effects, directional hydrogen bonding, and coordination interactions or π - π stacking.^{12–14} For instance, Stupp and co-workers have studied a series of glycopeptides that orthogonally self-assemble into nanofibers driven by hydrogen bonding and hydrophobic effects, showing high potential application in the stabilization of growth factors and bone regeneration.¹⁵ Brunsveld and co-workers developed a mannose functionalized discotic molecule that can copolymerize to form supramolecular polymers with tunable bacterial aggregation efficacy.¹⁶ We have previously synthesized a library of benzene-1,3,5-tricarboxamide (BTA)-based supramolecular

Received: June 21, 2019

Published: August 7, 2019

Scheme 1. Synthesis Pathways of the BTA-Saccharides^a

^a(A) BTA-Glc, BTA-Man, and BTA-Cel were synthesized by reacting BTA-C12-OH with participating imidate donors followed by deprotection with NaOMe. (B) BTA-OEG₄-Man was synthesized through glycosylation with 2,3,4,6-tetra-*O*-benzoyl- α -D-mannopyranosyl trichloroacetimidate to BTA-OEG₄ and followed by deprotection with NaOMe.

monomers that could be functionalized at their periphery via azide–alkyne click reactions with monosaccharides and showed that these could be used to generate fibrous assemblies in water, however without internal order.^{17,18}

The modular properties of supramolecular copolymerization in principle opens up endless possibilities to create new materials exhibiting enhanced complexities and functionalities.¹⁸ It is challenging however to achieve the subtle balance between the complementary recognizing motifs through noncovalent heterointeractions in supramolecular copolymers. Although some elegant examples have been reported in organic solvents, e.g., kinetically controlled living supramolecular copolymers,^{19–22} only limited aqueous examples have been reported so far. Manners and co-workers have published seminal contributions on crystalline driven supramolecular copolymerization in aqueous solution, resulting in various morphologies in a living fashion.^{23,24} Oppositely charged polypeptide supramolecular monomers were demonstrated by Besenius and co-workers to copolymerize into fibrous structures at neutral pH, whereas they disassembled at low and high pH.²⁵

In our continued efforts toward revealing the underlying mechanisms and structure-kinetics-function relationship on supramolecular (co)polymerization in water, we have explored a BTA-based platform that undergoes supramolecular (co)-polymerization to yield different nanostructures.^{26–28} The most extensively studied monomer is BTA-OEG₄ (Scheme

1B) bearing a tetraethylene glycol as periphery, that self-assembles into micrometers long nanofibers driven by hydrophobic effects and intermolecular hydrogen bonding. Most recently, we showed that a dendronized BTA (dBTA), which does not self-assembles by itself, can be copolymerized with BTA-OEG₄ into a more stable nanofibrous structure exhibiting slower exchange dynamics for both monomers as compared to the individual assemblies.²⁷ This copolymerization approach provides opportunities to build architectures with controlled dynamics and functional group distributions at the periphery, and the possibility to generate hydrogels with tunable mechanical properties at higher concentrations. Today, most of the hydrogels developed contain poly(ethylene glycol) for water-solubility, which may limit *in vivo* applications and lacks the option for functionalization.^{30–32} Carbohydrates can serve as alternatives allowing water solubility and providing means for tailored cell recognition. In order to control the dynamics, functionality, and stability of the carbohydrate-based supramolecular polymers, new avenues have to be discovered to construct complex multicomponent supramolecular glycopolymers.

Herein, by taking advantage of a modular supramolecular (co)assembly methodology, a variety of saccharide functionalized supramolecular polymers and copolymers are generated, incorporating different carbohydrates of high interest for further biological applications. A family of saccharide functionalized BTA-based monomers is synthesized via acid catalyzed

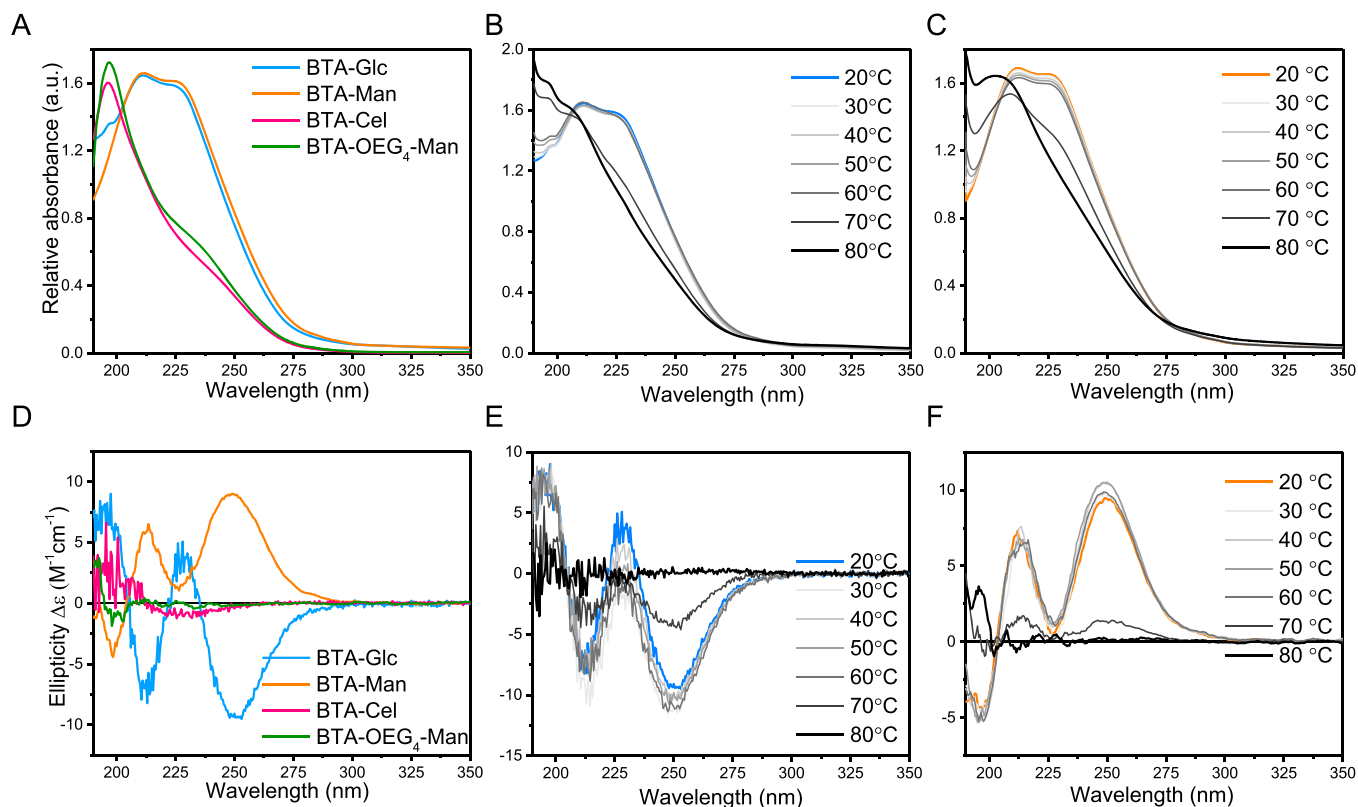


Figure 1. UV (A–C) and CD (D–F) spectra of the assembled individual molecules in water. (A) BTA-Glc and BTA-Man in water show the typical BTA maxima at 211 and 225 nm, whereas BTA-Cel and BTA-OEG₄-Man show maxima at 196 nm. (B) and (C) Stepwise heating of BTA-Glc and BTA-Man, respectively, from 20 °C to 80 °C showed a change in aggregation between 60 °C and 70 °C for both of BTA-Glc and BTA-Man. (D) BTA-Glc and BTA-Man show a biphasic negative and positive mirror Cotton effect, whereas BTA-Cel and BTA-OEG₄-Man are CD silent. (E) and (F) Stepwise heating of BTA-Glc and BTA-Man, respectively, from 20 to 80 °C showed a drop in ellipticity between 60 °C and 80 °C. Samples were equilibrated for 16 min at the designated temperature to allow the formation of equilibrated aggregates. ($c_{\text{BTA}} = 50 \mu\text{M}$).

glycosylation installing monosaccharides (β -D-glucose, α -D-mannose) or a disaccharide (β -D-cellobiose) on the hydrophobic core (Scheme 1A). In addition a BTA-tetraethylene glycol was functionalized with an α -D-mannose to generate a monomeric building block having the carbohydrate further away from the BTA core. The saccharides presented at the periphery of the supramolecular structures are selected as possible antifouling saccharides (glucose and cellobiose) to reduce aspecific cell interactions, and their antimicrobial properties (mannose), possibly valuable for future cell experiments.³³ The homopolymerization and copolymerization behavior of the saccharide based monomeric building blocks has been elucidated in an aqueous environment, showing the critical role of the carbohydrate appendage for the self-assembly behavior and internal order, opening up avenues for biomaterial science.

RESULTS AND DISCUSSION

Molecular Design and Synthesis. A modular synthetic platform was developed to easily install different saccharides onto a BTA-based core using a glycosylation reaction. A hydrophobic alkyl linker of 12 carbons was selected to protect the inner 3-fold hydrogen bonds from water penetration and to drive assembly by a hydrophobic collapse. This length was previously proven to be the most optimal spacing for the ethylene glycol BTA (BTA-OEG₄) 1D fibrous assembly.³⁴ To this end, a C12 linker was attached to the benzene core with hydroxyl end groups at the periphery (BTA-C12-OH, Scheme

1A). For the glycosylation of D-glucose, D-mannose and D-cellobiose, reactive trichloroacetimidate donors protected with participating benzoyl esters were selected to achieve glycosylations with high 1,2-trans stereoselectivity.³⁵ The solubility of the starting material in conventional glycosylation solvents was too low to allow for productive reactions and hexafluoro-*iso*-propanol was found optimal for the condensation reactions. Notably, because of the low nucleophilicity of the protic solvent, minimal hexafluoro-*iso*-propyl glycosides were formed. Next, the protecting groups were removed to yield BTA- β -D-glucose (BTA-Glc), BTA- α -D-mannose (BTA-Man), and BTA- β -D-cellobiose (BTA-Cel) in 31%, 45%, and 12% overall yield, respectively (Scheme 1A). Similarly, as shown in Scheme 1B, BTA-OEG₄ was used as precursor for the synthesis of BTA-OEG₄- α -D-mannose (BTA-OEG₄-Man) via direct glycosylation, with an overall yield of 56%. The integrity and purity of the BTA structures were confirmed by ¹H NMR, ¹³C NMR, FT-IR spectroscopy, matrix assisted laser desorption ionization-time-of-flight mass spectrometry (MALDI-TOF-MS), and liquid chromatography–mass spectrometry (LC-MS) analysis (Figures S21–26 of the Supporting Information, SI).

Assembly of BTA-Glc, BTA-Man, BTA-Cel, and BTA-OEG₄-Man. We first studied the supramolecular homopolymerization of BTA-Cel and BTA-OEG₄-Man in MQ water at pH 6.4, using a previously described preparation protocol.³⁴ To this end BTA-saccharide powder was weighed in a vial and dissolved in MQ water, after which the samples were vortexed,

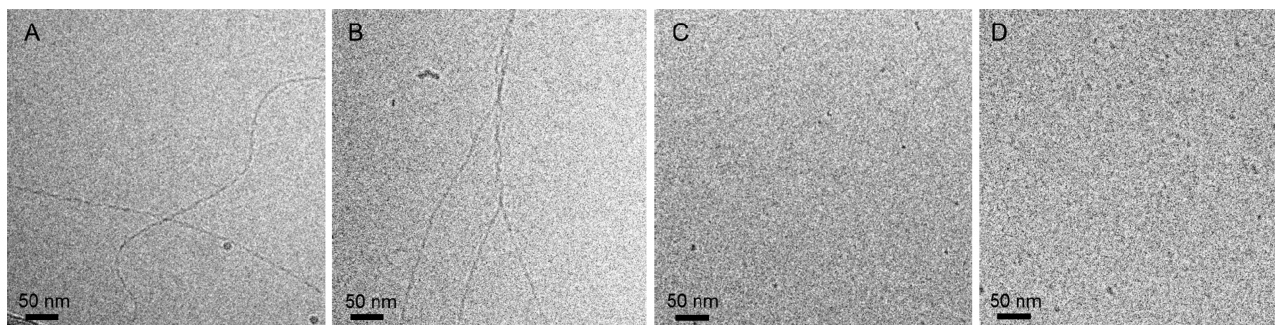


Figure 2. Cryo-TEM of BTA-Glc (A), BTA-Man (B), BTA-Cel (C), and BTA-OEG₄-Man (D). Micrometers long fibrous structures were observed for BTA-Glc and BTA-Man while micellar structures for BTA-Cel and BTA-OEG₄-Man. Scale bars indicate 50 nm, $c_{\text{BTA}} = 250$ or $500 \mu\text{M}$.

heated, vortexed, and allowed to assemble at room temperature, followed by equilibration overnight prior to measuring. This protocol, however, was not suitable for BTA-Glc and BTA-Man, since large particles were unable to reach the (sub)molecular dissolved state in water at high temperatures,^{36,37} and therefore, injection from a cosolvent was required. Thus, BTA-Glc or BTA-Man was dissolved in methanol to obtain a concentrated stock solution, which was subsequently injected into MQ water. After overnight equilibration, dialysis against MQ water was performed to remove the methanol content. The pH of the assembled BTA-saccharide samples was about 7 and remained stable over time.

To investigate the resulting supramolecular polymers, the samples were probed by UV spectrophotometry. Both the BTA-Glc and BTA-Man showed two absorption maxima at 211 and 225 nm (Figure 1A) similar to the BTA-OEG₄ previously reported, and indicative of a fibrous assembly.²⁸ The UV spectrum of the BTA-Glc or BTA-Man upon heating remained similar until 60 °C, whereas at 70 °C, a different spectrum was recorded with a broad maximum at lower wavelengths (Figure 1B and 1C) suggesting disassembly at this temperature. In contrast, BTA-Cel and BTA-OEG₄-Man in water showed an absorption maximum at 196 nm (Figure 1A), which gradually shifted to 198 upon heating (Figure S1). A similar absorbance at around 197 nm was also observed for the previously reported dBTA, which was shown to form spherical micelles instead of 1D nanofibers.²⁹ The UV spectra of the BTA-Glc, BTA-Man, BTA-Cel, and BTA-OEG₄-Man thus suggest different assemblies, with the first two forming 1D assemblies, and the latter two generating smaller micellar aggregates. In line with these findings, continuous heating UV experiments and micro-DSC heating experiments showed clear disassembly temperatures for the BTA-Glc and BTA-Man assemblies, which were absent in the BTA-Cel and BTA-OEG₄-Man samples (Figures S2 and S3).

Although the peripheral saccharides are situated far from the hydrogen bonding core, we observed a preference in helicity upon assembly by employing circular dichroism (CD) spectroscopy. The CD spectra of BTA-Cel and BTA-OEG₄-Man in water showed a negligible CD profile (Figure 1D). In contrast, a biphasic Cotton effect with minima at 211 and 250 nm was observed for BTA-Glc and a mirror image biphasic Cotton effect for BTA-Man. The CD profile of BTA-Glc is similar to that of the CD of a chiral α -deuterium BTA-fiber previously reported.³⁴ As depicted in Figure 1E and 1F, the CD pattern remained similar upon heating, with a sudden drop in intensity at 70 °C and became gradually CD silent at 80 °C.

This temperature behavior supports the UV measurements, indicating stable structures up to 60 °C.

Static light scattering (SLS) was performed to further inform on potential supramolecular architectures. SLS measures the scattering intensity as a dependence of the scattering angle, which can provide information about size, shape, and molar mass of the particles. In the BTA-Glc and BTA-Man samples, an angle dependent scattering intensity was observed, indicating elongated structures (Figure S4). In contrast, BTA-Cel and BTA-OEG₄-Man showed low scattering intensities at all angles and an absence of angular dependency, indicating small spherical-like aggregation.

Subsequently, cryogenic transmission electron microscopy (cryo-TEM) was employed to obtain structural information on the assemblies. Micrometers long fibers for BTA-Glc and BTA-Man were observed, with a diameter between 5 and 10 nm (Figure 2A and 2B), whereas small micelles of ca. 5 nm in size for BTA-Cel and BTA-OEG₄-Man were detected (Figure 2C and 2D). Detailed analysis shows in some cases a periodic feature due to twisting or aggregation; a detail that needs further studies. BTA-Man formed bundled fibers as shown in Figure 2B, possibly as a result of mannose–mannose interactions.^{36,37} Self-assembly and accompanied bundling occurred within seconds, whereas increased order developed over hours (Figure S5). Occasionally, a few (bundled) fibers were observed in the BTA-Cel sample as well, but these were not representative for the content of the sample. Altogether, these data show that BTA-Glc and BTA-Man assemble into 1D nanofibers, whereas BTA-Cel and BTA-OEG₄-Man do not, indicating that fiber formation is a subtle balance between hydrophobic to hydrophilic ratio, steric effects of the carbohydrates and carbohydrate-carbohydrate interactions.³⁸

Finally, the exchange dynamics of the monomers within the homopolymers was investigated by employing hydrogen/deuterium exchange mass spectrometry (HDX-MS), previously utilized in our group.^{17,26,30} This label-free method allows the determination of solvent exchanged monomers, due to an increase in molecular weight as a result of deuterium exchange of the hydrogen atoms in hydroxyls and amines. Upon contact with deuterated water, outer hydroxyl groups readily exchange, whereas the three inner amides exchange simultaneously upon monomer migration. Concentrated stock solutions of homopolymers (500 μM or 250 μM in the case of BTA-Man, due to the instability at higher concentration) were prepared in H₂O and subsequently diluted 100 times in D₂O, after which mass spectra through electrospray ionization mass spectrometry (ESI-MS) were collected as a function of time. As expected, all hydroxyl groups exchanged to OD immediately after dilution

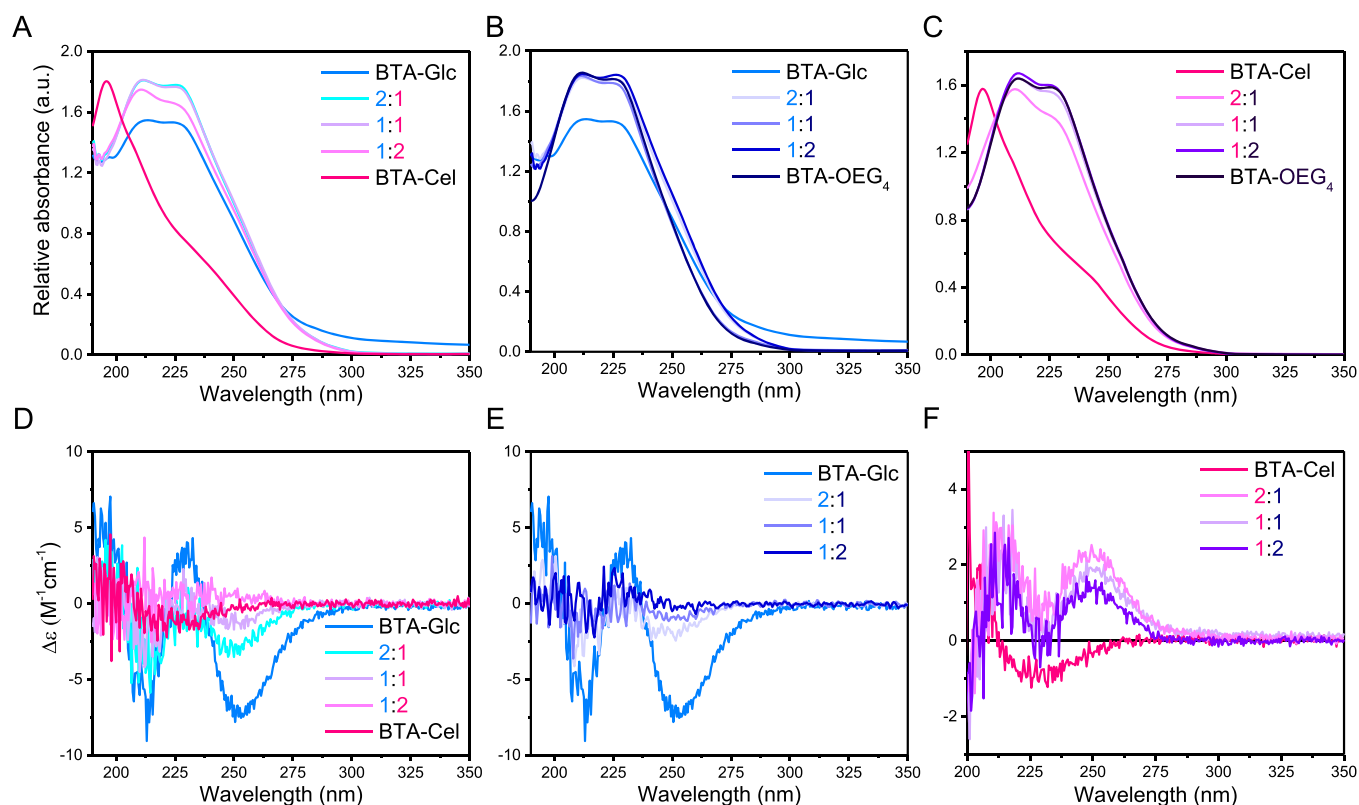


Figure 3. UV (top) and CD (bottom) spectra of coassembled BTAs in water at 20 °C. (A) and (D) BTA-Glc coassembled with BTA-Cel. (B) and (E) BTA-Glc coassembled with BTA-OEG₄. (C) and (F) coassembly of BTA-Cel with BTA-OEG₄. CD spectra of BTA-OEG₄ were discarded due to a large LD effect. Note that the 1:2 Glc:OEG₄ mixture displayed a small negative LD effect. ($c_{\text{BTA, total}} = 50 \mu\text{M}$).

into D₂O, whereas the well protected inner NH groups in BTA-Man and BTA-Glc exchanged gradually (Figure S6). Similar to the BTA-OEG₄, the data could be fitted with a triexponential fit, indicating monomers with different mobilities. The fit of BTA-Man followed a slower decay as compared to BTA-OEG₄, demonstrating more rigid and stable aggregates. In contrast, BTA-Cel and BTA-OEG₄-Man were instantaneously fully deuterated indicating a very weak or absent supramolecular ordered structure, substantiating the findings described above.

Coassembly of BTA-Glc, BTA-Man, BTA-Cel, BTA-OEG₄-Man and BTA-OEG₄. To generate supramolecular polymers having the β -D-cellobiose, β -D-glucose or α -D-mannose exposed at the periphery in different densities, we next turned to the generation of copolymers to fully explore the scope of the modular BTA-saccharides approach. First, the supramolecular copolymerization of BTA-Cel or BTA-OEG₄-Man was explored with the monomers that are capable of generating stable fibers, BTA-Glc, BTA-Man or BTA-OEG₄. To this end coassembled structures were prepared by mixing the individual assembled stocks in a 2:1, 1:1, or 1:2 ratio, following the assembly preparation protocol described above. Co-assembling BTA-Cel and BTA-Glc resulted in the typical absorption maxima at 211 and 225 nm (Figure 3A), indicating the successful copolymerization into fibrous structures. The corresponding CD-spectra showed a decrease in ellipticity with increasing BTA-Cel content, suggesting less well-ordered conformations in the supramolecular copolymer (Figure 3D). BTA-Cel copolymerized with BTA-OEG₄ also provided similar UV spectra (Figure 3C), whereas the corresponding CD-spectra showed a reversed biphasic Cotton effect as compared

to BTA-Glc, which changed only moderately with changing monomer ratio. Of note, the chirality of this helix is opposite to that of the polymer, even though the chirality of the appendages, consisting both of β -D-glucose-type moieties, is similar. The stable CD effect of the BTA-Cel/BTA-OEG₄ copolymers suggests that stable fiber can be formed as a result of the proper lateral alignment between the cellobiose moieties, which cannot be attained in structures composed of solely BTA-Cel monomers.^{39–42} The coassembly of BTA-Glc with BTA-OEG₄ again showed a similar UV-absorption profile (Figure 3B), with a significant loss of chirality (Figure 3E). Assemblies formed by BTA-OEG₄ showed a large CD and LD (linear dichroism) effect, probably due to a macroscopic orientation rather than due to chirality,^{36,37} therefore, the CD spectra of the BTA-OEG₄ were not used for analyses. The LD signal in all other samples was small and therefore had a minimal influence on the CD (Figure S7).

In order to further investigate the coassembled aggregates, the existence of a hydrophobic pocket was investigated using a Nile red fluorescence assay.³⁸ In water, Nile red shows very low fluorescence at around 665 nm (Figure S8A–C), while in contact with a hydrophobic environment an increase in fluorescence with a blue shift of the maximum is detected. At a total BTA concentration of 50 μM , all measured samples showed a blue shift to around 615 nm, with an increase in fluorescence intensity as compared to Nile red in water, thus indicative of a hydrophobic pocket. No significant differences between the homo- and copolymers could be deduced from the assay.

Next, SLS measurements of the mixtures were performed to investigate the aggregation size in more detail. All mixtures

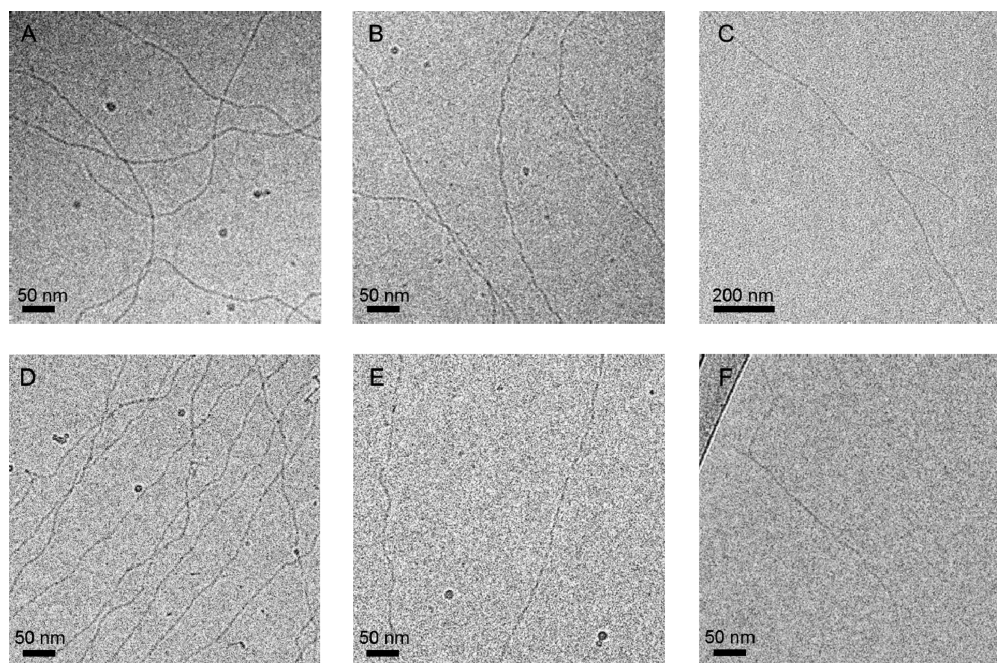


Figure 4. Cryo-TEM of 1:1 mixtures. (A) Glc: Cel, (B) Glc: OEG₄, (C) Cel: OEG₄, (D) OEG₄-Man: OEG₄, (E) Man: OEG₄, and (F) Man: OEG₄-Man. (C) TEM without staining. Fibrous structures and micelles were observed. $c_{\text{BTA}} = 500 \mu\text{M}$.

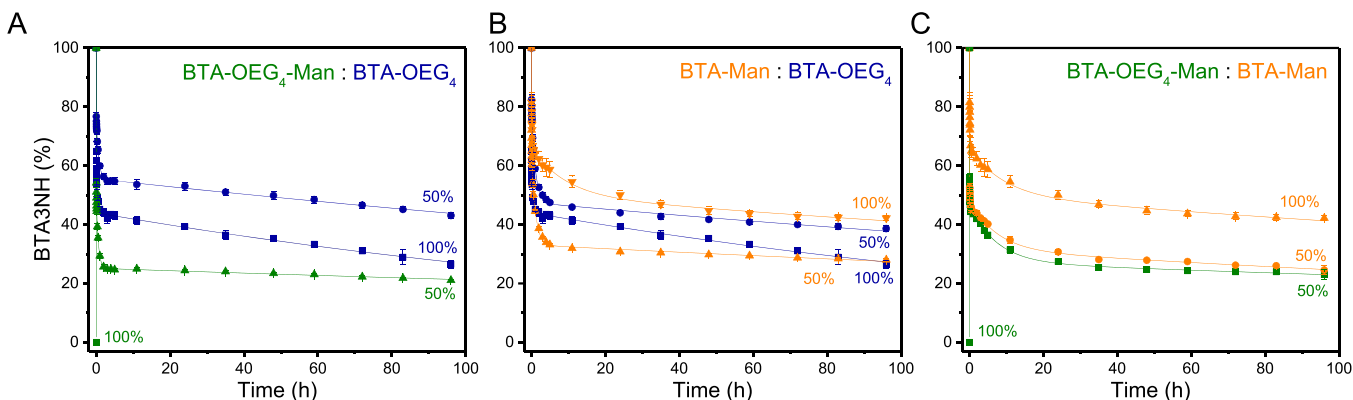


Figure 5. HDX-MS curves of homopolymers and copolymers (1:1 ratio) after 100 times dilution into D₂O. The graphs highlight the amount of remaining unexchanged monomers (BTA3NH) as a function of time. (A) BTA-OEG₄-Man coassembled with BTA-OEG₄, (B) BTA-Man with BTA-OEG₄, and (C) BTA-OEG₄-Man and BTA-Man. The data was fitted with a triexponential fit. $c_{\text{BTA}} = 5 \mu\text{M}$.

showed similar aggregation size as compared to BTA-OEG₄, further supporting the formation of fibrous assemblies (Figure S8D–F). In addition, small-angle X-ray scattering (SAXS) was employed for the BTA-Cel assemblies with and without BTA-OEG₄. The SAXS profile of the BTA-Cel, incapable of forming fibers by itself, displayed a plateau at lower q values, indicating small spherical-like particles, whereas the BTA-Cel: BTA-OEG₄ coassemblies showed a slope at lower q , indicating long fibrous structures (Figure S9). The dimensions obtained from the fits of the SAXS data corroborate well with the dimensions measured in cryo-TEM (Figure 4) and TEM of the 1:1 BTA-Cel: BTA-OEG₄ (Figure 4C). Cryo-TEM of the other 1:1 mixtures (BTA-Glc: BTA-Cel and BTA-Glc: BTA-OEG₄) also showed micrometers long fibrous structures and in some cases a periodic feature was observed similar as that of the homopolymers. These data show that BTA-Cel monomers are able to coassemble with BTA-OEG₄ and BTA-Glc monomers to form 1D supramolecular fibrous structures instead of self-sorting into individual aggregates.

The influence of aging on the self-assembled structures was investigated since this may enhance the helical order as a result of improved packing over time. Most of the samples investigated did not show a difference in UV and CD upon aging the samples for 2 months, except for the mixtures BTA-Cel: BTA-OEG₄ (1:1) and BTA-Glc: BTA-Cel (1:1) (Figure S10). In the case of BTA-Cel: BTA-OEG₄, the chirality was slightly enhanced (Figure S10B). In contrast, BTA-Glc: BTA-Cel went from a CD silent profile at day 1, to a CD profile displaying a Cotton effect after 2 months. LD did not affect this behavior (Figure S10C). This indicates slow readjustments into a more stable supramolecular conformation exhibiting a strong CD effect highlighting the need for careful alignment to induce helical order.

Overall, the data clearly show that all studied copolymerizations led to 1D assemblies. The highest induction of optical activity, hence indicating the highest order in the helical aggregate, is observed for the BTA-Glc homopolymers, which decreased when coassembled with BTA-Cel and which almost

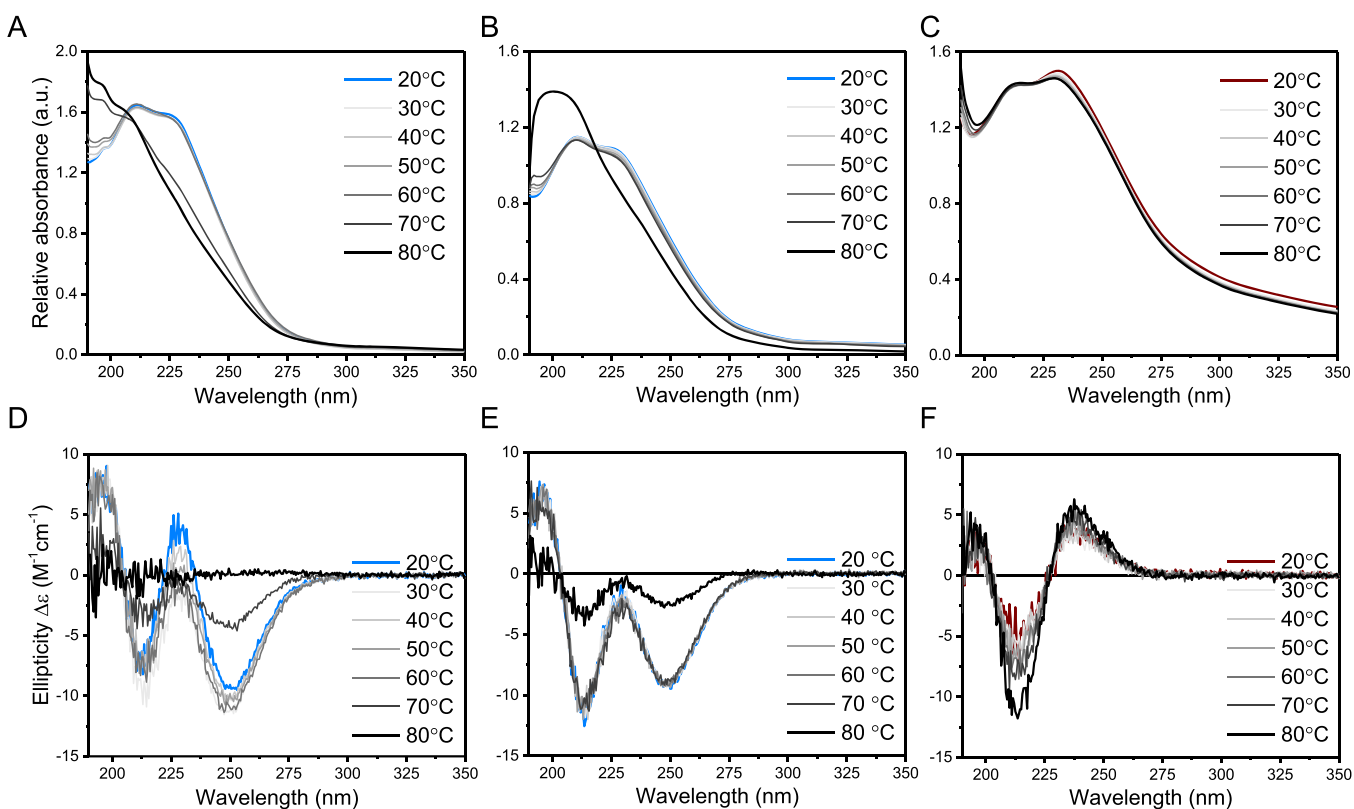


Figure 6. Influence of purities on BTA-Glc assembly. A–C indicates UV spectra and D–F CD spectra. (A) and (D) pure BTA-Glc showing a transition between 60 and 70 °C. (B) and (E) 85% BTA-3Glc mixed with 15% BTA-2Glc showing disassembly at 80 °C. (C) and (F) BTA-2Glc revealing a stability beyond 80 °C. Samples were equilibrated for 16 min at the designated temperature to allow the formation of equilibrated aggregates. ($c_{\text{BTA}} = 50 \mu\text{M}$).

vanished when copolymerized with BTA-OEG₄. In contrast, the coassembly of BTA-Cel with BTA-OEG₄ showed an induction of optical activity with a similar CD intensity for all the mixtures measured. The reduction in CD intensity might be the result of induced steric hindrance when the more bulky BTA-Cel is incorporated in BTA-Glc, thereby disordering the fiber backbone.

Similarly, the supramolecular copolymerization of BTA-Man, BTA-OEG₄-Man, and BTA-OEG₄, as well as BTA-Glc with BTA-Man at different mixing ratios of 2:1, 1:1, and 1:2 was investigated with UV, CD, SLS (Figures S11–14) and cryo-TEM (Figure 4D–F). Combined, these techniques proved the formation of 1D micrometers long fibers with diameters of ca. 8 nm. The exchange dynamics of the copolymers (1:1 ratio) were monitored by HDX-MS, revealed different monomer exchange profiles for all mixtures measured (Figures 5 and S15). This substantiates the successful copolymerization, since self-sorting would result in similar exchange profiles as the homopolymers (Figure 5, 50% compared to their 100% counterpart). Upon copolymerizing BTA-OEG₄-Man with BTA-OEG₄ a slower monomer exchange as compared to their 100% counterpart is observed (Figure 5A), suggesting a stabilization effect upon coassembly. This stabilization behavior was previously observed when dBTA was copolymerized with BTA-OEG₄.²⁷ In contrast, an increased monomer exchange was observed when BTA-Man was copolymerized with either BTA-OEG₄ or BTA-OEG₄-Man (Figure 5B and 5C), suggesting a destabilizing effect. In other words by copolymerization of different comonomers, the exchange dynamics of BTA-Man can be tuned.

The Influence of Sample Preparation and Purity on Self-Assembly.

During these studies we were confronted with subtleties that are worth publishing. The sample preparation method is critical in the assembly to avoid undesirable kinetic traps and is key to reproducibility. As mentioned in the paragraph on homopolymerization, BTA-Glc and BTA-Man require a cosolvent to allow assembly to occur since the carbohydrate–carbohydrate interactions in the solid are too strong to be disrupted by solely water addition and thermal energy. Interestingly, when BTA-Glc was mixed with 15% of the 2-armed BTA-Glc—unforeseen encountered with a less pure sample—water solubility was readily obtained without the need for a cosolvent. Not only the water solubility has changed, also the CD pattern was different (Figure 6E) as compared to pure BTA-Glc (Figure 6D). Contrary, the assemblies were shown to be more stable at higher temperatures, since the transition temperature for disassembly was shifted from 60 °C to 70–80 °C (Figures 6A, 6B, and S16). Allowing the 2-armed BTA-Glc to self-assemble in water revealed an even higher thermal stability reaching beyond 80 °C, although precipitation was observed by scattering at higher wavelengths (Figure 6C). Co-assembling the mixture of BTA-Glc (85% BTA-3Glc, 15% BTA-2Glc) with BTA-Cel or BTA-OEG₄ (Figure S17) showed subtle differences in UV and CD patterns as well as compared to copolymerized pure BTA-Glc (Figure 3A and 3B). Moreover, solubility and self-assembly in buffer was investigated as well (Figure S18). BTA-Glc and BTA-Man in phosphate buffered saline (PBS) precipitated, whereas BTA-Cel and BTA-OEG₄-Man readily dissolved, although the latter did not self-assemble into 1D fibers. In

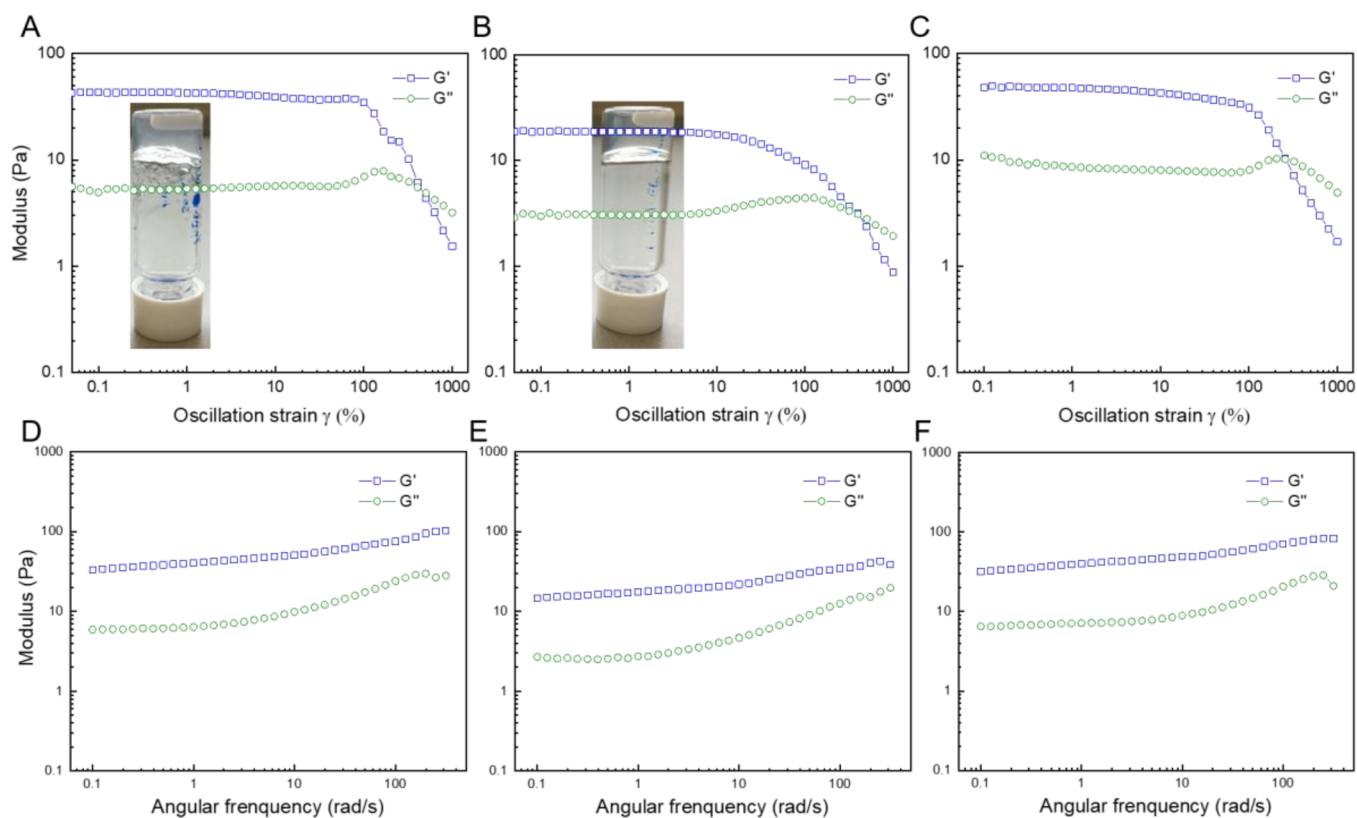


Figure 7. Rheology measurements of 5 wt % hydrogels formed by BTA-Man: BTA-OEG₄ (1:2, **HG1**, A,D), BTA-OEG₄-Man: BTA-OEG₄ (1:2, **HG2**, B,E), and BTA-Glc: BTA-OEG₄ (1:2, **HG3**, C,F) at 37 °C showing the storage and loss moduli (G' , G''). (A–C) Strain dependent oscillatory rheology (fixed angular frequency of 1 rad/s) with a photograph of the inverted vial containing the corresponding hydrogel in the inset. (D–F) Frequency sweep measurements (fixed applied strain of 1%).

contrast, all copolymers did dissolve and form elongated assemblies in buffer similar to their counterparts in pure water. These results highlight that the composition of the samples have not only a profound effect on the water and buffer solubility but also on the nanoscopic ordering of the structure, hence studying copolymers is highly important in understanding complex assembly processes.

Hydrogel Formation. The formation of hydrogels was investigated with selected copolymers capitalizing on the fiber entanglement, most strongly observed for the BTA-Glc fibers. Hydrogel formation of BTA-Man with BTA-OEG₄ (1:2, **HG1**), BTA-OEG₄-Man with BTA-OEG₄ (1:2, **HG2**) and BTA-Glc with BTA-OEG₄ (1:2, **HG3**) was optimized starting from the sample preparation protocol described above. Fast cooling in an ice bath after heating and vortexing proved to be necessary to form a more transparent hydrogel (5 wt %) as compared to cooling at room temperature. The mechanical properties of the hydrogels were investigated by rheological measurements. Strain dependent oscillatory rheology of the hydrogels displayed a linear region with a larger storage modulus (G') as compared to the loss modulus (G'') indicating a viscoelastic material (Figure 7). Moreover, a gel-to-sol transition was observed upon 400% strain (Figure 7A–C). Viscoelastic hydrogels were formed in all cases with low storage moduli resulting in extremely soft gels ($G'_{\text{HG1}} \approx 42$ Pa, $G'_{\text{HG2}} \approx 20$ Pa and $G'_{\text{HG3}} \approx 47$ Pa). The storage modulus of **HG1** and **HG3** are similar when compared to hydrogels formed from BTA-OEG₄ (Figure S19), whereas **HG2** shows lower mechanical properties. The anticipated self-healing

properties of the hydrogels were investigated in step-strain measurements revealing fast recovery (Figure S20).

These initial proof-of-concept experiments show that by carefully selecting monomers, hydrogels can be fabricated with specific functionalities due to supramolecular copolymerization. Although the prepared hydrogels are extremely weak, it is anticipated that the mechanical properties can be further enhanced by increasing the wt % or including cross-links. Together with their self-healing properties, their modular approach and the option to be modified with specific carbohydrates at the periphery, these supramolecular hydrogels are very attractive candidates for biomedical applications, e.g., the culture of soft tissues.

CONCLUSIONS

Inspired by the various functions of polysaccharides present in the glycocalyx and the extracellular matrix, biomaterials based on poly- and oligosaccharides have been previously developed. Here, BTA-based supramolecular polymers presenting mono- (β -D-glucose and α -D-mannose) and disaccharides (β -D-cellobiose) at the periphery were developed as ethylene glycol substitutes previously described and interrogated on their self-assembly properties using several techniques. A combination of UV, CD, light scattering and cryo-TEM proved to be powerful in elucidating the aggregation behavior into great detail. BTA-Glc and BTA-Man self-assembled into chiral 1D helical supramolecular polymers. In contrast, BTA-Cel and BTA-OEG₄-Man formed small spherical-like assemblies instead. Probably due to the bulky and highly hydrophilic character of BTA-Cel and BTA-OEG₄-Man, spherical micelles are favored

over 1D fibers. In contrast, coassembling BTA-Cel or BTA-OEG₄-Man with BTA-Glc, BTA-Man, or BTA-OEG₄ resulted in 1D fibrous supramolecular copolymers with BTA-Cel or BTA-OEG₄-Man incorporated in the supramolecular copolymers. Interestingly, chirality was induced upon mixing BTA-Cel with BTA-OEG₄, in contrast to a reduction or even suppression of chirality when BTA-Glc was copolymerized with BTA-Cel or BTA-OEG₄. This highlights that the chiral order of the supramolecular aggregates is the result of careful packing of the peripheral chiral saccharides and not due directly to the cooperative effect of the core. The supramolecular structures generated and investigated here provide a deeper understanding of supramolecular copolymerization—an area with many unknowns to be discovered—and taught us that subtle changes in monomer structure, preparation, and aging can have a profound effect on the packing of the monomers as well as their stability in time. In future experiments the mechanical properties in the gel state can be further tuned by controlling the weight percentage and ratio of different BTA-based monomers, and more functionality can be incorporated by mixing in, e.g., peptide functionalized BTAs. Carefully selecting monomers in supramolecular copolymerization opens avenues to fabricate endless variants of multi-component functional polymeric materials, having functionalities that are not accessible in supramolecular homopolymers.

■ ASSOCIATED CONTENT

■ Supporting Information

The Supporting Information is available free of charge on the ACS Publications website at DOI: 10.1021/jacs.9b06607.

Materials and instrumentation, synthetic procedures and characterizations, methods, and supporting figures (PDF)

■ AUTHOR INFORMATION

Corresponding Author

*e.w.meijer@tue.nl

ORCID

Simone I. S. Hendrikse: 0000-0002-8902-613X

Lu Su: 0000-0001-8207-756X

René P. M. Lafleur: 0000-0003-0026-3428

Jeroen D. C. Codee: 0000-0003-3531-2138

E. W. Meijer: 0000-0003-4126-7492

Author Contributions

[§]S.I.S.H. and L.S. contributed equally to this work.

Funding

The authors declare no competing financial interest.

Notes

The authors declare no competing financial interest.

■ ACKNOWLEDGMENTS

This work was funded by the NWO/DPI program NEWPOL (project #731.015.503), partially financed with TKI (Top-consortia for Knowledge Innovation) allowance provided by the Dutch Ministry of Economic Affairs, and by the Ministry of Education, Culture, and Science (Gravity program FMS, 024.001.035 and Gravity program ICI, 024.002.009).

■ REFERENCES

- (1) Reitsma, S.; Slaaf, D. W.; Vink, H.; Van Zandvoort, M. A. M. J.; Oude Egbrink, M. G. A. The Endothelial Glycocalyx: Composition, Functions, and Visualization. *Pfluegers Arch.* **2007**, *454* (3), 345–359.
- (2) Köwitsch, A.; Zhou, G.; Groth, T. Medical Application of Glycosaminoglycans: A Review. *J. Tissue Eng. Regener. Med.* **2018**, *12* (1), 23–41.
- (3) Mouw, J. K.; Ou, G.; Weaver, V. M. Extracellular Matrix Assembly: A Multiscale Deconstruction. *Nat. Rev. Mol. Cell Biol.* **2014**, *15* (12), 771–785.
- (4) Gandhi, N. S.; Mancera, R. L. The Structure of Glycosaminoglycans and Their Interactions with Proteins. *Chem. Biol. Drug Des.* **2008**, *72* (6), 455–482.
- (5) Shelke, N. B.; James, R.; Laurencin, C. T.; Kumbar, S. G. Polysaccharide Biomaterials for Drug Delivery and Regenerative Engineering. *Polym. Adv. Technol.* **2014**, *25* (5), 448–460.
- (6) Mammen, M.; Choi, S.-K.; Whitesides, G. M. Polyvalent Interactions in Biological Systems: Implications for Design and Use of Multivalent Ligands and Inhibitors. *Angew. Chem., Int. Ed.* **1998**, *37* (20), 2754–2794.
- (7) Freudenberg, U.; Liang, Y.; Kiick, K. L.; Werner, C. Glycosaminoglycan-Based Biohybrid Hydrogels: A Sweet and Smart Choice for Multifunctional Biomaterials. *Adv. Mater.* **2016**, *28* (40), 8861–8891.
- (8) Lutz, J. F.; Lehn, J. M.; Meijer, E. W.; Matyjaszewski, K. From Precision Polymers to Complex Materials and Systems. *Nat. Rev. Mater.* **2016**, *1* (5) DOI: 10.1038/natrevmats.2016.24.
- (9) Célia Monteiro de Paula, R.; Andrade Feitosa, J.; Beserra Paula, H. Polysaccharide Based Copolymers as Supramolecular Systems in Biomedical Applications. *Curr. Drug Targets* **2015**, *16* (14), 1591–1605.
- (10) Webber, M. J.; Appel, E. A.; Meijer, E. W.; Langer, R. Supramolecular Biomaterials. *Nat. Mater.* **2016**, *15* (1), 13–26.
- (11) Meyers, M. A.; Chen, P.-Y.; Lin, A. Y.-M.; Seki, Y. Biological Materials: Structure and Mechanical Properties. *Prog. Mater. Sci.* **2008**, *53* (1), 1–206.
- (12) De Greef, T. F. A.; Smulders, M. M. J.; Wolffs, M.; Schenning, A. P. H. J.; Sijbesma, R. P.; Meijer, E. W. Supramolecular Polymerization. *Chem. Rev.* **2009**, *109* (11), 5687–5754.
- (13) Goor, O. J. G. M.; Hendrikse, S. I. S.; Dankers, P. Y. W.; Meijer, E. W. From Supramolecular Polymers to Multi-Component Biomaterials. *Chem. Soc. Rev.* **2017**, *46* (21), 6621–6637.
- (14) Straßburger, D.; Stergiou, N.; Urschbach, M.; Yurugi, H.; Spitzer, D.; Schollmeyer, D.; Schmitt, E.; Besenius, P. Mannose-Decorated Multicomponent Supramolecular Polymers Trigger Effective Uptake into Antigen-Presenting Cells. *ChemBioChem* **2018**, *19* (9), 912–916.
- (15) Lee, S. S.; Fyrner, T.; Chen, F.; Álvarez, Z.; Sleep, E.; Chun, D. S.; Weiner, J. A.; Cook, R. W.; Freshman, R. D.; Schallmo, M. S.; Katchko, K. M.; Schneider, A. D.; Smith, J. T.; Yun, C.; Singh, G.; Hashmi, S. Z.; McClendon, M. T.; Yu, Z.; Stock, S. R.; Hsu, W. K.; Hsu, E. L.; Stupp, S. I. Sulfated Glycopeptide Nanostructures for Multipotent Protein Activation. *Nat. Nanotechnol.* **2017**, *12* (8), 821–829.
- (16) Müller, M. K.; Brunsveld, L. A Supramolecular Polymer as a Self-Assembling Polyvalent Scaffold. *Angew. Chem., Int. Ed.* **2009**, *48* (16), 2921–2924.
- (17) Leenders, C. M. A.; Jansen, G.; Frissen, M. M. M.; Lafleur, R. P. M.; Voets, I. K.; Palmans, A. R. A.; Meijer, E. W. Monosaccharides as Versatile Units for Water-Soluble Supramolecular Polymers. *Chem. - Eur. J.* **2016**, *22* (13), 4608–4615.
- (18) Schoenmakers, S. M. C.; Leenders, C. M. A.; Lafleur, R. P. M.; Lou, X.; Meijer, E. W.; Pavan, G. M.; Palmans, A. R. A. Impact of the Water-Compatible Periphery on the Dynamic and Structural Properties of Benzene-1,3,5-Tricarboxamide Based Amphiphiles. *Chem. Commun.* **2018**, *54* (79), 11128–11131.
- (19) Makam, P.; Gazit, E. Minimalistic Peptide Supramolecular Co-Assembly: Expanding the Conformational Space for Nanotechnology. *Chem. Soc. Rev.* **2018**, *47* (10), 3406–3420.

- (20) Mukhopadhyay, R. D.; Ajayaghosh, A. Living Supramolecular Polymerization. *Science (Washington, DC, U. S.)* **2015**, *349* (6245), 241–242.
- (21) Rugar, P. A.; Chabanne, L.; Winnik, M. A.; Manners, I. Non-Centrosymmetric Cylindrical Micelles by Unidirectional Growth. *Science (Washington, DC, U. S.)* **2012**, *337* (6094), 559–562.
- (22) Görl, D.; Zhang, X.; Stepanenko, V.; Würthner, F. Supramolecular Block Copolymers by Kinetically Controlled Co-Self-Assembly of Planar and Core-Twisted Perylene Bisimides. *Nat. Commun.* **2015**, *6* (1), 7009.
- (23) Hill, J. P.; Jin, W.; Kosaka, A.; Fukushima, T.; Ichihara, H.; Shimomura, T.; Ito, K.; Hashizume, T.; Ishii, N.; Aida, T. Self-Assembled Hexa-Peri-Hexabenzocoronene Graphitic Nanotube. *Science (Washington, DC, U. S.)* **2004**, *304* (5676), 1481–1483.
- (24) Nazemi, A.; Boott, C. E.; Lunn, D. J.; Gwyther, J.; Hayward, D. W.; Richardson, R. M.; Winnik, M. A.; Manners, I. Monodisperse Cylindrical Micelles and Block Comicelles of Controlled Length in Aqueous Media. *J. Am. Chem. Soc.* **2016**, *138* (13), 4484–4493.
- (25) Finnegan, J. R.; He, X.; Street, S. T. G.; Garcia-Hernandez, J. D.; Hayward, D. W.; Harniman, R. L.; Richardson, R. M.; Whittell, G. R.; Manners, I. Extending the Scope of “Living” Crystallization-Driven Self Assembly: Well-Defined 1D Micelles and Block Comicelles from Crystallizable Polycarbonate Block Copolymers. *J. Am. Chem. Soc.* **2018**, *140* (49), 17127–17140.
- (26) Frisch, H.; Unsleber, J. P.; Lüdeker, D.; Peterlechner, M.; Brunklaus, G.; Waller, M.; Besenius, P. PH-Switchable Ampholytic Supramolecular Copolymers. *Angew. Chem., Int. Ed.* **2013**, *52* (38), 10097–10101.
- (27) Matsumoto, N. M.; Lafleur, R. P. M.; Lou, X.; Shih, K. C.; Wijnands, S. P. W.; Guibert, C.; Van Rosendaal, J. W. A. M.; Voets, I. K.; Palmans, A. R. A.; Lin, Y.; Meijer, E. W. Polymorphism in Benzene-1,3,5-Tricarboxamide Supramolecular Assemblies in Water: A Subtle Trade-off between Structure and Dynamics. *J. Am. Chem. Soc.* **2018**, *140* (41), 13308–13316.
- (28) Thota, B. N. S.; Lou, X.; Bochicchio, D.; Paffen, T. F. E.; Lafleur, R. P. M.; van Dongen, J. L. J.; Ehrmann, S.; Haag, R.; Pavan, G. M.; Palmans, A. R. A.; Meijer, E. W. Supramolecular Copolymerization as a Strategy to Control the Stability of Self-Assembled Nanofibers. *Angew. Chem., Int. Ed.* **2018**, *57* (23), 6843–6847.
- (29) Leenders, C. M. A.; Albertazzi, L.; Mes, T.; Koenigs, M. M. E.; Palmans, A. R. A.; Meijer, E. W. Supramolecular Polymerization in Water Harnessing Both Hydrophobic Effects and Hydrogen Bond Formation. *Chem. Commun.* **2013**, *49* (19), 1963–1965.
- (30) Armstrong, J. K.; Hempel, G.; Kolling, S.; Chan, L. S.; Fisher, T.; Meiselman, H. J.; Garratty, G. Antibody against Poly(Ethylene Glycol) Adversely Affects PEG-Asparaginase Therapy in Acute Lymphoblastic Leukemia Patients. *Cancer* **2007**, *110* (1), 103–111.
- (31) Richter, A. W.; Åkerblom, E. Polyethylene Glycol Reactive Antibodies in Man: Titer Distribution in Allergic Patients Treated with Monomethoxy Polyethylene Glycol Modified Allergens or Placebo, and in Healthy Blood Donors. *Int. Arch. Allergy Immunol.* **2004**, *74* (1), 36–39.
- (32) Pelegri-O'Day, E. M.; Lin, E.-W.; Maynard, H. D. Therapeutic Protein-Polymer Conjugates: Advancing beyond Pegylation. *J. Am. Chem. Soc.* **2014**, *136* (41), 14323–14332.
- (33) Ham, H. O.; Park, S. H.; Kurutz, J. W.; Szleifer, I. G.; Messersmith, P. B. Antifouling Glycocalyx-Mimetic Peptoids. *J. Am. Chem. Soc.* **2013**, *135* (35), 13015–13022.
- (34) Lou, X.; Lafleur, R. P. M.; Leenders, C. M. A.; Schoenmakers, S. M. C.; Matsumoto, N. M.; Baker, M. B.; van Dongen, J. L. J.; Palmans, A. R. A.; Meijer, E. W. Dynamic Diversity of Synthetic Supramolecular Polymers in Water as Revealed by Hydrogen/Deuterium Exchange. *Nat. Commun.* **2017**, *8*, 15420.
- (35) Wu, X.; Su, L.; Chen, G.; Jiang, M. Deprotection-Induced Micellization of Glycopolymers: Control of Kinetics and Morphologies. *Macromolecules* **2015**, *48* (11), 3705–3712.
- (36) Dashnau, J. L.; Sharp, K. A.; Vanderkooi, J. M. Carbohydrate Intramolecular Hydrogen Bonding Cooperativity and Its Effect on Water Structure. *J. Phys. Chem. B* **2005**, *109* (50), 24152–24159.
- (37) Carcabal, P.; Jockusch, R. A.; Hunig, I.; Snoek, L. C.; Kroemer, R. T.; Davis, B. G.; Gambelin, D. P.; Compagnon, I.; Oomens, J.; Simons, J. P. Hydrogen Bonding and Cooperativity in Isolated and Hydrated Sugars: Mannose, Galactose, Glucose, and Lactose. *J. Am. Chem. Soc.* **2005**, *127* (32), 11414–11425.
- (38) Lombardo, D.; Kiselev, M. A.; Magazù, S.; Calandra, P. Amphiphiles Self-Assembly: Basic Concepts and Future Perspectives of Supramolecular Approaches. *Adv. Condens. Matter Phys.* **2015**, *2015*, 1–22.
- (39) Bucior, I.; Burger, M. M. Carbohydrate-Carbohydrate Interactions in Cell Recognition. *Curr. Opin. Struct. Biol.* **2004**, *14* (5), 631–637.
- (40) Narushima, T.; Okamoto, H. Circular Dichroism Microscopy Free from Commingling Linear Dichroism via Discretely Modulated Circular Polarization. *Sci. Rep.* **2016**, *6* (1), 35731.
- (41) Huang, X.; Li, C.; Jiang, S.; Wang, X.; Zhang, B.; Liu, M. Self-Assembled Spiral Nanoarchitecture and Supramolecular Chirality in Langmuir-Blodgett Films of an Achiral Amphiphilic Barbituric Acid. *J. Am. Chem. Soc.* **2004**, *126*, 1322–1323.
- (42) Sackett, D. L.; Wolff, J. Nile Red as a Polarity-Sensitive Fluorescent Probe of Hydrophobic Protein Surfaces. *Anal. Biochem.* **1987**, *167* (2), 228–234.